

Enhancing operational wind downscaling capabilities over Canada: Application of a Conditional Wasserstein GAN methodology

Jorge Guevara¹, Victor Nascimento¹, Johannes Schmude¹, Daniel Salles¹, Simon Corbeil-Létourneau², Madalina Surcel², and Dominique Brunet²

¹IBM Research

²Environment and Climate Change Canada

Abstract

Wind downscaling is essential for improving the spatial resolution of weather forecasts, particularly in operational Numerical Weather Prediction (NWP). This study advances wind downscaling by extending the DownGAN framework introduced by Annau et al. to operational datasets from the Global Deterministic Prediction System (GDPS) and High-Resolution Deterministic Prediction System (HRDPS), covering the entire Canadian domain. We enhance the model by incorporating high-resolution static covariates, such as HRDPS-derived topography, into a Conditional Wasserstein Generative Adversarial Network with Gradient Penalty, implemented using a UNET-based generator. Following the DownGAN framework, our methodology integrates low-resolution GDPS forecasts (15 km, 10-day horizon) and high-resolution HRDPS forecasts (2.5 km, 48-hour horizon) with Frequency Separation techniques adapted from computer vision. Through robust training and inference over the Canadian region, we demonstrate the operational scalability of our approach, achieving significant improvements in wind downscaling accuracy. Statistical validation highlights reductions in root mean square error (RMSE) and log spectral distance (LSD) metrics compared to the original DownGAN. High-resolution conditioning covariates and Frequency Separation strategies prove instrumental in enhancing model performance. This work underscores the potential for extending high-resolution wind forecasts beyond the 48-hour horizon, bridging the gap to the 10-day low resolution global forecast window.

1 Introduction

Accurate high-resolution wind forecasts are crucial for several application sectors such as aviation [1], wind energy [2], power infrastructure [3], public safety [4], wildfire management [5], avalanche warnings [6], winter sports [7], air quality [8] and water quality management [9]. Typically, wind forecasts are obtained from numerical weather predictions (NWP), starting with a global forecast model followed by a limited-area forecast model which takes the lower-resolution model as boundary conditions in a procedure called dynamical downscaling. In Canada, high-resolution numerical prediction models have a limited forecast horizon of 48 hours due to computational constraints. An applied perspective of the work presented in this paper is to extend high-resolution wind forecast services from 48 hours to the same 10 days forecast horizon as the Canadian global forecast model.

In meteorology, downscaling is the operation of passing from a coarse (or low-resolution) field to a fine (or high-resolution) field. Besides dynamical downscaling, statistical downscaling is another well established approach for correcting wind at station locations. Several variations of Model Output Statistics (MOS) [10,11] have been proposed in the literature, with the Updateable Model Output Statistics (UMOS) [12] approach the one implemented operationally at Environment and climate Change Canada (ECCC). All the MOS techniques are essentially based on the concept of Multiple Linear Regression (MLR), where several predictors from the lower-resolution NWP output are combined linearly to minimize the mean square error against an observed weather field, with one specific model used at each station location. MOS techniques can be expanded to gridded fields as long as a high-resolution gridded target is available, or specific corrections applied at each station can be interpolated to the grid [13], but they cannot capture complex non-linear spatial interactions between variables.

More recently, several contributions have demonstrated the potential of Artificial Intelligence (AI) based downscaling [14–25], applying successfully techniques originally developed for image processing and computer vision to weather data. In the field of image processing, the image super-resolution (or zooming) problem consists of taking a coarser image as input and producing a finer image at higher resolution.¹

Earlier methods were achieving an enhancement factor of 2 to 4 times, but with the advent of deep learning, an enhancement factor of 8 and more is now possible. Generative AI in particular has proven to be a powerful tool not only to artificially produce realistic-looking images and videos from a random seed, but also to condition the generative AI on coarser or partially missing data (called inpainting).

AI-based techniques for downscaling weather and climate fields can be classified in an increasing order of complexity and recency. At the end of spectrum, ensemble decision trees techniques such random forests and extreme gradient

¹Confusingly, what is called upsampling (downsampling) in the field of image processing is called downscaling (upsampling) in meteorology.

boosting are the most similar to MLR and the easiest to implement. Other classical machine learning techniques such as support vector machine and shallow artificial neural networks with a single hidden layer can also fit in that category. Methods based on Convolutional Neural Networks (CNNs) have proved to be both popular and powerful. Generative Adversarial Networks (GANs) are the first type of generative AI allowing to sample an ensemble of possible realizations [15]. More recently, latent diffusion techniques have emerged as an interesting alternative to GAN. Finally, methods based on vision transformers and in particular those that consist of fine-tuning a weather foundation model are emerging.

In the literature, these methods have been applied to a variety of weather fields such as temperature, wind speed or wind vectors, and precipitation. Many of the published work focus on one or several small areas as a proof-of-concept, and few are used in an operational setting. It is important to note that similar AI techniques can be used either for downscaling weather forecasts, climate projections or reanalysis data, with the main difference in the choice and resolution of source and target data. Moreover, with a general downscaling model, there is no conceptual difference between downscaling to a finer grid or downscaling to a point location that could be either an existing weather station or any location of interest.

The key contributions of this work are as follows: 1) We extend the DownGAN framework introduced by [15] by applying its methods to operational Numerical Weather Prediction (NWP) datasets, specifically GDPS and HRDPS across the entire Canadian domain, expanding beyond the regional focus of the original study. 2) We enhance the DownGAN model, a Wasserstein GAN with Gradient Penalty (WGAN-GP) framework for wind downscaling, by introducing high-resolution static covariates, such as topography from the HRDPS domain, as conditioning inputs within the generator architecture, implemented using a UNET. We refer this modified framework as a Conditional WGAN-GP. 3) We propose a robust training and inference schema that allows the model to effectively learn wind patterns and generate predictions over the entire Canadian region. This development ensures the scalability and operational relevance of the methodology. 4) We perform statistical validation for large-scale wind downscaling across the Canadian domain, identifying limitations such as the ineffectiveness of Annau’s partial frequency separation technique in this context. However, Frequency Separation methods adapted from computer vision and used by DownGAN show strong performance. The validation highlights the importance of high-resolution conditioning covariates and the utility of Frequency Separation in this context.

The paper is divided as follows. Section 2 introduces the datasets and the pre-processing steps in preparation for training the AI model. Section 3 presents the methods for training and inference of the AI model. Experimental results follow in Section 4, and Discussion and Conclusions are presented in Section 5.

2 Dataset

2.1 Global Deterministic Prediction System

The Global Deterministic Prediction System (GDPS) [26] is ECCC’s operational long-range forecast model. It represents the global configuration of the Global Environmental Multiscale (GEM) model [27] and it is run twice a day (at 00 UTC and 12 UTC), producing 10-day forecasts at a 15-km nominal resolution.

2.2 High-Resolution Deterministic Prediction System

The High-Resolution Deterministic Prediction System (HRDPS) [28] is a limited-area model (LAM) configuration of GEM for Canada and Northern United States. The prediction is run operationally at ECCC every 6 hours (00 UTC, 06 UTC, 12 UTC and 18 UTC runs) for a 48 hours forecast at 2.5-km nominal resolution. The HRDPS is the main source of NWP guidance for the Meteorological Service of Canada for day 1 and day 2 forecasts.

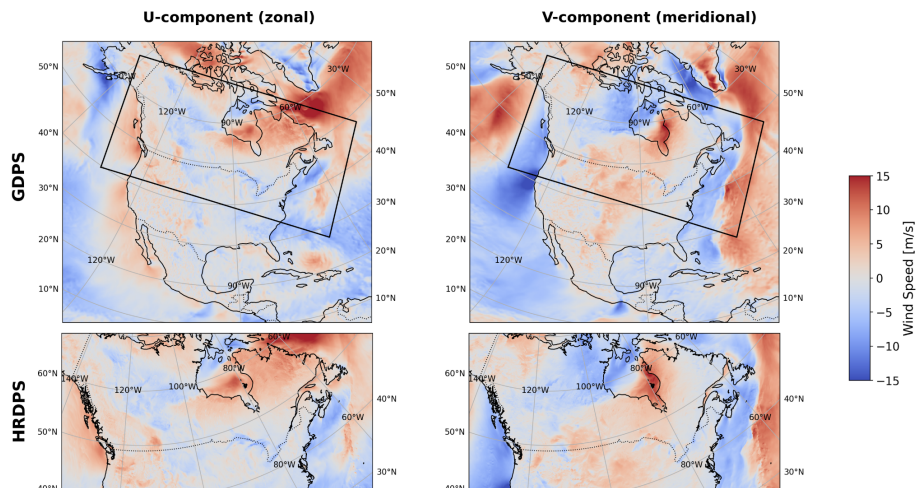


Figure 1: GDPS and HRDPS

2.3 Predictors and Predictands

High-resolution zonal (East-West) and meridional (North-South) surface (10 m) wind components from HRDPS are used as the target variables. By predicting both components of the wind vector, we can derive both wind speed and direction at the resolution of HRDPS. Low-resolution zonal and meridional surface wind from GDPS are taken as predictors along with surface temperature, as well as wind, temperature and vertical motion at 546 hPa. In contrast with [15], high-resolution geophysical fields are added as predictors. These

static high-resolution covariates can be used as predictors since these variables are constant at the time-scale of weather prediction. The topography field is particularly important in mountainous regions where wind channeling is predominant. The land-water mask not only provides an indication of changing surface roughness between the smoother water and other land, but can also be a driver of local winds such as sea breezes and lake breezes. Finally, the surface roughness variable modulates the speed of the wind and changing surface roughness can drive turbulence in the planet boundary layer. Table 1 describes the meteorological variables used for training the AI downscaling model.

Table 1: Description of Variables for GDPS and HRDPS

Description
GDPS Predictors
True geographical West-East (zonal) component of the horizontal wind at the surface (10 m) [m/s].
True geographical South-North (meridional) component of the horizontal wind at the surface (10 m) [m/s].
Air temperature at the surface (1.5 m) [°C].
Air temperature vertically interpolated at 546 hPa [°C].
True geographical West-East (zonal) component of the horizontal wind vertically interpolated at 546 hPa [m/s].
True geographical South-North (meridional) component of the horizontal wind vertically interpolated at 546 hPa [m/s].
Vertical motion vertically interpolated at 546 hPa [Pa/s].
HRDPS Predictands
True geographical West-East (zonal) component of the horizontal wind at the surface (10 m) [m/s]. Denoted by u10.
True geographical South-North (meridional) component of the horizontal wind at the surface (10 m) [m/s]. Denoted by v10.
HRDPS Static Covariates
Model orography [m].
Water/land mask [fraction].
Roughness length [m].

2.4 Data Pre-processing

The map projection of the GDPS outputs is a Yin-Yang grid with a different rotated latitude-longitude map projection than the one of the HRDPS grid. We regrid the GDPS grid to the HRDPS grid using nearest neighbor interpolation. The interpolated data is then reduced by a factor of 8 (20-km nominal resolution) as the input of the AI downscaling method. Fig.1 illustrates the respective domains of GDPS (cropped over North-America) and of HRDPS.

3 Methods

In this study, we adopt the deep learning framework for downscaling wind components proposed by [15]. This framework is based on Wasserstein Generative Adversarial Networks with Gradient Penalty (WGAN-GP) [29] and incorporates elements from Generative Adversarial Networks for image super-resolution (SRGAN) [30] as a baseline for the downscaling task. In the following sections, we elaborate on the application of WGANs for the downscaling problem, describe the model architecture, and introduce our approach to integrating high-resolution static covariates into the training process using UNETs [31].

3.1 Conditional WGAN-GP for Downscaling

Given a training set consisting of dynamic low-resolution (GDPS) and high-resolution (HRDPS) forecast hours, denoted as \mathbf{x} and \mathbf{y} , respectively. A conditional WGAN-GP, conditioned on the covariates \mathbf{y}_{cov} in the HRDPS domain, aims to minimize the following losses for the critic \mathcal{L}_C and generator \mathcal{L}_G [15, 29, 32]:

$$\mathcal{L}_C = \mathbb{E}_{G(\mathbf{x}) \sim \mathbb{P}_g} [C(G(\mathbf{x} | \mathbf{y}_{\text{cov}}))] - \mathbb{E}_{\mathbf{y} \sim \mathbb{P}_r} [C(\mathbf{y})] + \lambda \mathbb{E}_{\hat{\mathbf{y}} \sim \mathbb{P}_{\hat{y}}} [(\|\nabla_{\hat{y}} C(\hat{y})\|_2 - 1)^2] \quad (1)$$

$$\mathcal{L}_G = -\gamma \mathbb{E}_{G(\mathbf{x}) \sim \mathbb{P}_g} [C(G(\mathbf{x} | \mathbf{y}_{\text{cov}}))] + \alpha \mathbb{E}_{\mathbf{y} \sim \mathbb{P}_r} l_c(\mathbf{y}, G(\mathbf{x} | \mathbf{y}_{\text{cov}})) \quad (2)$$

In this formulation, C denotes a real-valued function known as the *Critic*, which is defined on the HRDPS domain. The function G represents the *Generator*, which maps low-resolution GDPS to the HRDPS domain. The symbol \mathbb{P}_g denotes the conditional distribution of the generated downscaled GDPS data given the covariates \mathbf{y}_{cov} , while \mathbb{P}_r represents the distribution of the HRDPS points. The expression $\mathbb{E}_{\hat{\mathbf{y}} \sim \mathbb{P}_{\hat{y}}} [(\|\nabla_{\hat{y}} C(\hat{y})\|_2 - 1)^2]$ represents the *gradient penalty*, which is incorporated into the formulation to ensure valid Wasserstein distances by enforcing 1-Lipschitz continuity for the Critic. Here, $\hat{\mathbf{y}} \sim \mathbb{P}_{\hat{y}}$ denotes a linearly interpolated generated value defined by $\hat{\mathbf{y}} = \epsilon \mathbf{y} + (1 - \epsilon) G(\mathbf{x} | \mathbf{y}_{\text{cov}})$, where $\epsilon \sim U[0, 1]$. The scalars λ , γ , and α are regularization hyperparameters: λ controls the gradient penalty term, γ the adversarial loss term, $\mathbb{E}_{G(\mathbf{x}) \sim \mathbb{P}_g} [C(G(\mathbf{x} | \mathbf{y}_{\text{cov}}))]$ and α the content loss term, $\mathbb{E}_{\mathbf{y} \sim \mathbb{P}_r} l_c(\mathbf{y}, G(\mathbf{x} | \mathbf{y}_{\text{cov}}))$. All expectations in the equations above are computed across all dimensions of \mathbf{x} and \mathbf{y} . Specifically, \mathbf{x} is a tensor of size $B \times C_l \times W_l \times H_l$, and \mathbf{y} is a tensor of size $B \times C_h \times W_h \times H_h$. Here, B represents the batch size, W and H denote the spatial width and height, respectively, while C indicates the number of input channels (variates). The subscripts l and h refer to the GDPS and HRDPS datasets, respectively. Additionally, \mathbf{y}_{cov} is a tensor with dimensions $C_{\text{cov}} \times W_l \times H_l$, where values are replicated across the batch size B . This replication is due to the covariates being *static* and independent of time. It is important to note that if \mathbf{y}_{cov} is not provided, the WGAN-GP model reduces to the formulation presented in [15].

Utilizing WGAN-GP for downscaling is preferred over traditional GANs due to the advantages offered by WGANs. These advantages include a more stable training process and the provision of meaningful loss metrics, which contribute

to achieving better generative outputs. Additionally, WGAN-GP effectively mitigates common challenges encountered in GAN training, such as mode collapse and vanishing gradients. For a more comprehensive understanding of these concepts, please refer to the relevant literature [15, 29, 33].

3.1.1 Frequency Separation

The core idea of the frequency separation approach is to decompose the low- and high-frequency components and treat them differently during WGAN-GP training [15, 34], with the aim of enhancing the quality of downscaled wind components. This allows the adversarial training to focus specifically on generating the high-frequency components, which are crucial for capturing fine details. In this approach, the high-frequency components are derived as $\mathbf{y}_h = \mathbf{y} - H(\mathbf{y})$ for the HRDPS data, and $G(\mathbf{x} | \mathbf{y}_{\text{cov}})_h = G(\mathbf{x} | \mathbf{y}_{\text{cov}}) - H(G(\mathbf{x} | \mathbf{y}_{\text{cov}}))$ for the generated downscaled data, where H represents a low-pass filter. In this case, during WGAN-GP training, the Critic will focus on optimizing the loss based only in the high frequency components \mathbf{y}_h and $(G(\mathbf{x} | \mathbf{y}_{\text{cov}}))_h$ instead of \mathbf{y} and $(G(\mathbf{x} | \mathbf{y}_{\text{cov}}))$. On the other side the Generator delegates the generation of high frequency components to the adversarial component $-\mathbb{E}_{G(\mathbf{x})_h \sim \mathbb{P}_g}[C(G(\mathbf{x} | \mathbf{y}_{\text{cov}}))_h]$ and the low frequency components to the content loss $\mathbb{E}_{\mathbf{y} \sim \mathbb{P}_r} l_c(H(\mathbf{y}), H(G(\mathbf{x} | \mathbf{y}_{\text{cov}})))$. In [15] is proposed the partial frequency separation, this approach is similar than before but the adversarial loss is used in its original formulation, i.e., $-\mathbb{E}_{G(\mathbf{x}) \sim \mathbb{P}_g}[C(G(\mathbf{x} | \mathbf{y}_{\text{cov}}))]$

3.2 Architectures

3.2.1 Critic Network

To implement the proposed conditional WGAN-GP, we employed the same Critic network described by [15], as illustrated in Figure 2. The figure provides a schematic of the Critic network, with the numbers above each block indicating the dimensions of the data representations at various stages. The labels below the blocks denote the kernel size k , the number of filters n , and the stride s used in each layer. The Critic utilizes a VGG-style architecture that progressively reduces the spatial dimensions of the input, which may include HRDPS wind components or the downscaled version of GDPS wind components provided by the Generator network, through a sequence of convolutional layers. The network processes the input data using 3x3 convolutions with LeakyReLU activations, where each layer increases the number of feature maps while downsampling the spatial dimensions using a stride of 2. This approach allows the network to expand the number of channels up to eight times the input dimension. The extracted features are then passed through a final processing block, a regression-style scoring mechanism that reduces the feature vector to a single scalar output. This scalar score, used as an approximation of the Wasserstein distance, indicates the Critic’s assessment of how real the input data appears.

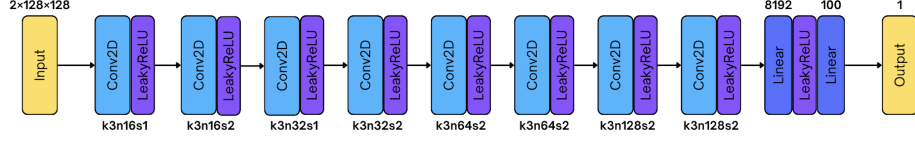


Figure 2: Schematic of the Critic Network

3.2.2 Generator Network

The generator network implemented in the proposed model draws upon concepts from [15, 30] and is structured according to a U-Net architecture. The architecture is depicted in Figure 3. We employ this design because it facilitates the integration of HRDPS covariates and GDPS variates as inputs. The Generator embeds the HRDPS covariates through a sequence of downsampling layers reducing the spatial dimensions by a factor of eight. The resulting output tensor is then concatenated with the feature map tensor derived from the GDPS variates. This combined tensor passes through a series of residual-in-residual dense blocks, for a deep feature extraction. Following this stage, the network employs a sequence of upsampling layers that utilize pixel shuffle operations, enabling the progressive restoration of spatial resolution. Throughout the upsampling process, skip connections from the downsampling layers are leveraged to facilitate the merging of local and global features while preserving high-frequency details. The final output layer incorporates a convolutional operation to generate the GDPS downscaled version of wind components. This U-Net architecture serves as the mechanism for implementing the conditional Wasserstein GAN, effectively utilizing HRDPS covariates to guide the generative process GDPS wind components.

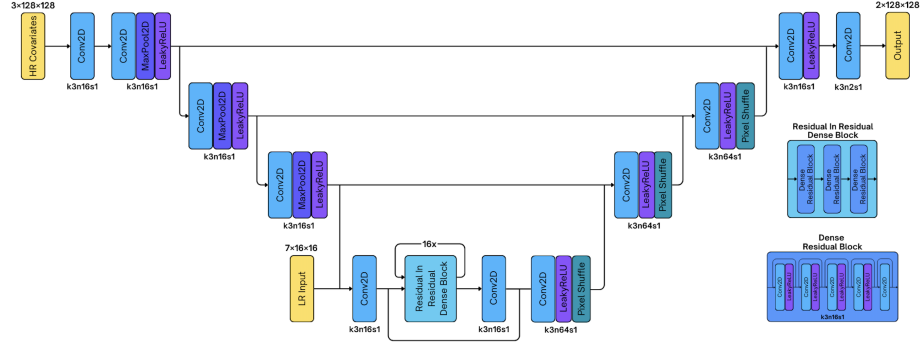


Figure 3: Schematic of the Generator Network

4 Experiments

4.1 Dataset Split

This section outlines the experimental setup, using a dataset of matched GDPS and HRDPS forecast hours. For each prediction system, 24 hours of forecasts are used for each day consisting of forecast lead-times 6-17 hours for each of the 00 and 12 UTC runs. In this way, we avoid both the model spin-up time, and later forecast times where the two systems might have diverged because of error growth. For training, we selected all GDPS and HRDPS files with predictions starting between July 2022 to June 2023. The dataset was randomly split into 7,150 files for training, 1,178 for validation, and 1,162 for testing.

4.2 Metrics

To evaluate the performance of the proposed conditional WGAN-GP, we used the Root Mean Squared Error (RMSE) between the HRDPS reference and the downscaled GDPS wind components. Additionally, we employed the Radially Averaged Log-Spectrum Distance (LSD) [19]:

$$LSD(\bar{P}_{true}, \bar{P}_{pred}) = \sqrt{\frac{1}{N_r} \sum_r \left(10 \log_{10} \frac{\bar{P}_{true}(r)}{\bar{P}_{pred}(r)} \right)^2}, \quad (3)$$

where $P(r)$ is the Radially Averaged Power Spectrum Density [19]. Observe that LSD quantifies the difference between predicted and true power spectra on a logarithmic scale. Subscripts $_{pred}$ and $_{true}$ are the $P(r)$ of predicted and true wind fields, respectively.

4.3 Training Procedures

The GDPS and HRDPS datasets cover the entire Canadian region. We applied a nearest-neighbor regridding approach to align the GDPS data with the HRDPS grid of (2540, 1280) spatial values, because each data set was provided in different rotated coordinate systems². We use this regridding because it preserves original pixel values avoiding interpolation artifacts. In this sense, each GDPS and HRDPS file is represented by tensors of sizes (7, 2540, 1280) and (2, 2540, 1280), where 7 and 2 represent the variable counts in GDPS and HRDPS, respectively, as detailed in Table 1. To train the WGAN-GP, we based our implementation in the open-source implementation from [36]. We used the following hyperparameters: *critic Iterations*: 5 (indicating one generator update per five critic updates), *batch size*: 32, *learning Rate*: 0.00025, *regularization hyperparameters*: $\lambda = 10$ (gradient penalty), $\gamma = 0.01$ (adversarial loss), and $\alpha = 5$ (content loss). We used spatial random cropping for training with a (128 × 128) crop size and a downsampling factor of 8 for the regridded GDPS, resulting in GDPS tensors of (7, 16, 16) for each corresponding HRDPS tensor of (2, 128, 128). We

²The regridding process was done using the xESMF Python Library [35]

generated 832 crops per GDPS/HRDPS pair, amounting to 5,948,800 random crops for the 7,150 pairs in the training dataset. Here, one "epoch" corresponds to using all 832 random crops from a single GDPS-HRDPS forecast hour. This random crop setup allows six generator updates using a batch size of 32.

The UNET generator network is configured with inputs of (32, 7, 16, 16) (batch size, variables, spatial dimensions) and receives an HRDPS static covariate tensor of (3, 128, 128). The generator produces tensors of (32, 2, 128, 128), representing the downscaled u10 and v10 wind components in the HRDPS domain. The critic network processes input tensors of (32, 2, 128, 128), derived from either HRDPS data or the downscaled GDPS output. The proposed conditional WGAN-GP was trained for 65,250 epochs, with validation involving 32 random crops per GDPS-HRDPS file in the validation set.

4.4 Effect of using HRDPS Static Covariates

In this experiment, we investigate the impact of incorporating HRDPS static covariates on downscaling accuracy. To this end, we compare the DownGAN model [15] using the open-source implementation from [36], against a the proposed conditional WGAN-GP that utilizes HRDPS covariates. Both models are trained with identical hyperparameters and configurations to ensure a fair comparison. The primary difference lies in their generator architectures: DownGAN employs a generator based on the SRGAN network introduced by [30], while the WGAN-GP model adapts the DownGAN generator to a UNET structure, allowing it to effectively incorporate the additional HRDPS covariates.

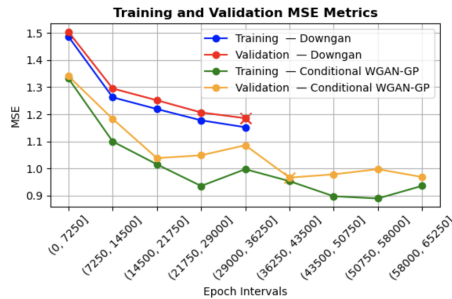


Figure 4: Training and validation curves: DownGAN vs conditional WGAN-GP

Figure 4 presents the MSE curve trajectories for the DownGAN and the Conditional WGAN-GP models across training and validation epochs. The MSE values are averaged over intervals of 7250 epochs, which correspond to the number of forecast hours in the training set. In the plot, the DownGAN model's training and validation MSE average values are represented by blue and red markers, respectively, while the Conditional WGAN-GP model's MSE average values are shown in green (training) and orange (validation). The Conditional WGAN-GP model, which incorporates HRDPS static covariates, demonstrates

consistently lower MSE values compared to the DownGAN model. The minimum validation MSE average value for each model is marked with an "x". The Conditional WGAN-GP model attains a lower validation error across all intervals, suggesting its enhanced capability for downscaling accuracy.

4.5 Effect of Frequency Separation

This section shows the experimental results to investigate the impact of Frequency Separation (FS) and Partial Frequency Separation (PFS) on the performance of the conditional WGAN-GP model. We tested multiple configurations for both FS and PFS, varying the low-pass average filter kernel sizes. Specifically, we used kernel sizes of (5, 5), (9, 9) and (13, 13) for each WGAN-GP model with FS and PFS. Additionally, we included a conditional WGAN-GP model without FS or PFS as a baseline (i.e., same MSE validation curve from Figure 4). For the experiments, we applied transfer learning starting from epoch 21,750, and continuing training up to epoch 50,750. Figure 5 presents a comparison of the models' performance based on the MSE validation metric.

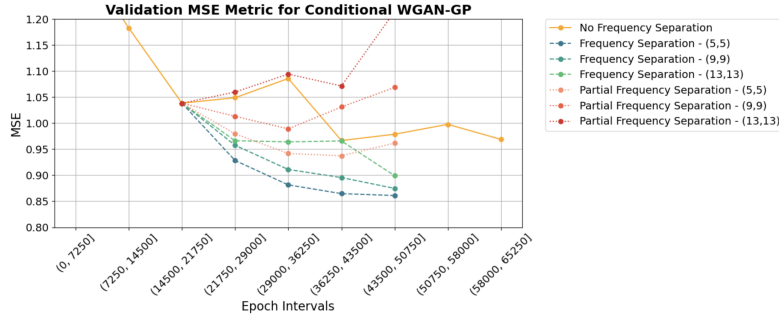


Figure 5: Effect of Frequency separation in the validation curve

From the experiments, we observed that FS is in general better than PFS, and that small filter kernel sizes are better in term of the validation MSE metric. For this experiment, WGAN-GP with FS achieved the best configuration using a filter size of (5, 5), obtaining an average MSE validation score of 0.86 in the interval [43500, 50750]. This result outperformed both the best PFS configuration (filter size of (5, 5) and MSE validation score of 0.93) and the case without frequency separation (MSE validation score of 0.97)

Figure 6 shows the effect of FS in dealing with high frequencies as a function of epochs 29000, 36250, 43500 and 50750. In this case, checkboard artifacts are less evident in WGAN-GP with FS than in the case with no frequency separation.

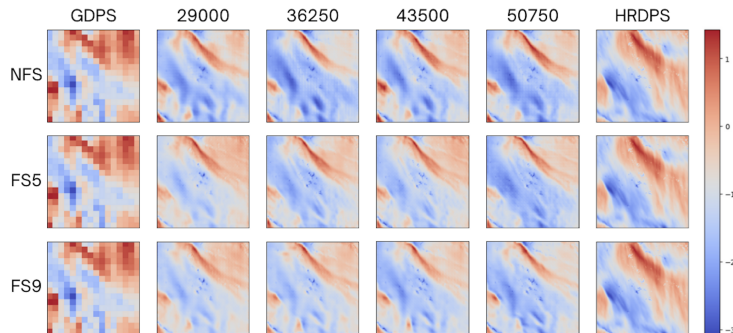


Figure 6: Effect of Frequency separation in downscaling at epoch 36250 — Left to right images: GDPS, GDPS downscaled with no frequency separation case, GDPS downscaled with WGAN-GP with FS using filter (7, 7) and HRDPS reference

4.6 Metrics on the Test Set

This section presents the metrics computed on a test set comprising 1,162 GDPS forecast hours. Figure 7 displays the results, contrasting the 1,162 downsampled GDPS forecast hours against HRDPS references in terms of RMSE and LSD metrics. We used Bilinear interpolation and nearest neighbor (NN) interpolation as baseline methods. Additionally, we evaluated several models, including the DownGAN model at checkpoint 29000, the Conditional WGAN-GP model at checkpoints 21,750 and 43,500 (no frequency separation scenario: NFS - 21,750 and NFS - 43,500, respectively), and the Conditional WGAN-GP model with frequency separation with kernels (13, 13), (9, 9) and (5, 5) at checkpoints 50,750 denoted by FS13 - 50,750, FS9 - 50,750, and FS5 - 50,750 respectively. The decision to select a specific model checkpoint was based on the lowest validation MSE metric (See experiments from Section 4.5). As shown by Figure 7, based on the test error in both metrics for the two wind components, the interpolation methods performed the worst. Additionally, the DownGAN model exhibited worse performance than the Conditional WGAN-GP variations. Among the Conditional WGAN-GP models, the method with frequency separation and a kernel size of 5, 5 provided the best performance in terms of the RMSE metric, and the one with kernel size of 9, 9 in terms of the LSD metric Table 2 presents a summary of the metrics on the test set in terms of their mean and standard deviation statistics.

Table 2: Summary of Results.

Method	RMSE (u10)		RMSE (v10)		LSD (u10)		LSD (v10)	
	Mean	Std	Mean	Std	Mean	Std	Mean	Std
DownGAN - 30000	0.953	0.333	0.904	0.305	2.287	1.223	2.327	1.292

Table 2: Summary of Results.

Method	RMSE (u10)		RMSE (v10)		LSD (u10)		LSD (v10)	
	Mean	Std	Mean	Std	Mean	Std	Mean	Std
FS13 - 50750	0.785	0.296	0.785	0.293	1.820	0.939	1.852	0.980
FS9 - 50750	0.771	0.298	0.764	0.286	1.755	0.914	1.671	0.887
FS5 - 50750	0.749	0.296	0.744	0.287	1.842	0.964	1.756	0.934
NFS - 43500	0.803	0.311	0.778	0.294	1.889	0.973	1.847	0.970
NFS - 21750	0.843	0.326	0.812	0.303	1.962	0.992	2.082	1.078
Bilinear	1.012	0.396	0.993	0.378	3.462	2.379	3.476	2.412
KNN	1.041	0.399	1.023	0.383	3.994	0.790	4.008	0.764

4.7 Inference over the whole Canadian Region

Downscaling is crucial for analyzing large geographical regions; however, memory constraints can arise due to factors such as spatial resolution, data quantity, and model size. To address this issue, downscaling is often performed on smaller regions or patches, which are then stitched together to create a larger image. To downscale wind components on the entire Canadian domain we used the conditional WGAN-GP to generate overlapping 128×128 images across the domain and then blend these overlapping areas using a weight matrix W , which is predefined 128×128 matrix with weights in the interval $[0, 1]$, increasing radially toward the center. Specifically, to generate a larger downscaling image I from smaller 128×128 images (patches), the algorithm starts by generating consecutive non-overlapping patches with a stride of 128 and copying the result directly into the corresponding region of I . Then, the entire region is again parsed, but this time the new patches overlap the artefacts. The final image is created by using linear interpolation between the patches generated in the last step and the correspondent pixels that were already in I by using the weight matrix W . Each value for pixel ij in image I' is given by $I'_{ij} = I_{ij} * (1 - W_{ij}) + \text{patch}_{ij} * W_{ij}$. Figure 8 provides a visual representation of this approach.

The top part of the figure highlights the region I , which contains artifacts and is constructed using consecutive non-overlapping patches. The bottom section illustrates how the inference overlapping algorithm generates and blends the new patches, constructing I' . It's important to note that the image of the entire Canada region is 2540×1280 , where both dimensions are not divisible by 128. As a result, the far right and bottom edges of the image contain regions that weren't filled. For these smaller regions, we generate additional patches and apply the Inference Overlapping Algorithm to fill in the remaining pixels.

5 Conclusions

In this study, we presented a downscaling methodology based on a conditional Wasserstein GAN (WGAN-GP), leveraging low-resolution data from the GDPS

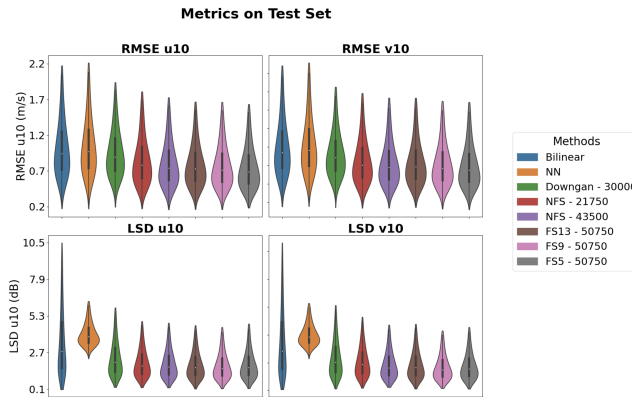


Figure 7: RMSE and LSD Metrics on the Test Set

and high-resolution data from the HRDPS, conditioned on high-resolution static covariates. We also conducted experiments incorporating the Frequency Separation approach to enhance the performance of the model. To implement the conditional WGAN-GP, we employed a UNET model as the generator. This UNET was designed to process two types of inputs: high-resolution static covariates and low-resolution GDPS data. Due to memory constraints, the training protocol relied on extracting random crops from single pairs of GDPS and HRDPS data. We carried out experiments to analyze the impact of including high-resolution static covariates in the model. Our findings indicate that these covariates significantly improved model convergence. Furthermore, experimental results demonstrated that the use of Frequency Separation contributed to further performance gains. We evaluated the generalization capability of the proposed model using a held-out test set. The results revealed that the best model configuration incorporated Frequency Separation, achieving favorable performance in terms of RMSE and Log Spectral Distance (LSD) metrics. To operationalize the model, we proposed a downscaling procedure for the entire Canadian domain. This procedure generates overlapping downscaled patches of size 128×128 and blends them into the larger Canadian region using a linear interpolation approach. As future work, we aim to operationalize the model as a product capable of extending high-resolution wind forecast services from the current 48-hour horizon to the 10-day forecast horizon of the Canadian global forecast model. Additionally, we plan to investigate the application of recent state-of-the-art weather foundation models [37] for wind downscaling.

References

- [1] Christopher M. Wynnyk. Wind analysis in aviation applications. In *2012 IEEE/AIAA 31st Digital Avionics Systems Conference (DASC)*, pages 5C2-1-5C2-10, October 2012.

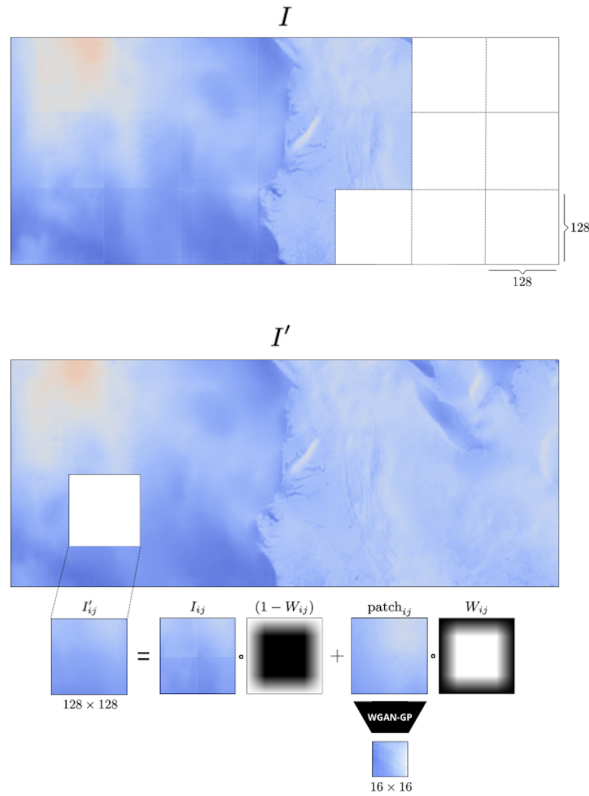


Figure 8: Inference overlapping strategy used to downscaling on the whole Canadian Region

- [2] Hao Chen. A novel wind model downscaling with statistical regression and forecast for the cleaner energy. *Journal of Cleaner Production*, 434:140217, January 2024.
- [3] Xiubing Huang and Naiyu Wang. An adaptive nested dynamic downscaling strategy of wind-field for real-time risk forecast of power transmission systems during tropical cyclones. *Reliability Engineering & System Safety*, 242:109731, February 2024.
- [4] Victoria A. Lang, Teresa J. Turner, Brandon R. Selbig, Austin R. Harris, and Jonathan D. W. Kahl. Predicting Peak Wind Gusts during Specific Weather Types with the Meteorologically Stratified Gust Factor Model. *Weather and Forecasting*, 37(8):1435–1446, August 2022.
- [5] Tom Beer. The interaction of wind and fire. *Boundary-Layer Meteorology*, 54(3):287–308, February 1991.

- [6] Michael Lehning and Charles Fierz. Assessment of snow transport in avalanche terrain. *Cold Regions Science and Technology*, 51(2):240–252, February 2008.
- [7] Hao Wang, Shuiqing Yin, Tianyu Yue, Xia Chen, and Deliang Chen. Developing a dynamic-statistical downscaling framework for wind speed prediction for the Beijing 2022 Winter olympics. *Climate Dynamics*, 62(8):7345–7363, August 2024.
- [8] Mohamed F. Yassin. Numerical modeling on air quality in an urban environment with changes of the aspect ratio and wind direction. *Environmental Science and Pollution Research*, 20(6):3975–3988, June 2013.
- [9] Dominique Brunet, Reza Valipour, and Yerubandi R. Rao. Wind variability over a large lake with complex topography: Lake of the Woods. *Journal of Great Lakes Research*, 49(1):112–121, February 2023.
- [10] Harry R. Glahn and Dale A. Lowry. The Use of Model Output Statistics (MOS) in Objective Weather Forecasting. *Journal of Applied Meteorology and Climatology*, 11(8):1203–1211, December 1972.
- [11] Joël Bédard, Wei Yu, Yves Gagnon, and Christian Masson. Development of a geophysic model output statistics module for improving short-term numerical wind predictions over complex sites. *Wind Energy*, 16(8):1131–1147, 2013.
- [12] Laurence J. Wilson and Marcel Vallée. The Canadian Updateable Model Output Statistics (UMOS) System: Design and Development Tests. *Weather and Forecasting*, 17(2):206–222, April 2002.
- [13] Bob Glahn, Kathryn Gilbert, Rebecca Cosgrove, David P. Ruth, and Kari Sheets. The Gridding of MOS. *Weather and Forecasting*, 24(2):520–529, April 2009.
- [14] Didit Adytia, Arnida L. Latifah, Deni Saepudin, Dede Tarwidi, Sri Redjeki Pudjaprasetya, Semeidi Husrin, Ardhasena Sopaheluwakan, and Gegar Prasetya. A deep learning approach for wind downscaling using spatially correlated global wind data. *International Journal of Data Science and Analytics*, September 2024.
- [15] Nicolaas J. Annau, Alex J. Cannon, and Adam H. Monahan. Algorithmic Hallucinations of Near-Surface Winds: Statistical Downscaling with Generative Adversarial Networks to Convection-Permitting Scales. *Artificial Intelligence for the Earth Systems*, December 2023.
- [16] Jorge Baño-Medina, Rodrigo Manzananas, and José Manuel Gutiérrez. Configuration and intercomparison of deep learning neural models for statistical downscaling. *Geoscientific Model Development*, 13(4):2109–2124, April 2020.

- [17] Jérôme Dujardin and Michael Lehning. Wind-Topo: Downscaling near-surface wind fields to high-resolution topography in highly complex terrain with deep learning. *Quarterly Journal of the Royal Meteorological Society*, 148(744):1368–1388, 2022.
- [18] Florian Dupuy, Pierre Durand, and Thierry Hedde. Downscaling of surface wind forecasts using convolutional neural networks. *Nonlinear Processes in Geophysics*, 30(4):553–570, November 2023.
- [19] Lucy Harris, Andrew T. T. McRae, Matthew Chantry, Peter D. Dueben, and Tim N. Palmer. A Generative Deep Learning Approach to Stochastic Downscaling of Precipitation Forecasts. *Journal of Advances in Modeling Earth Systems*, 14(10):e2022MS003120, 2022.
- [20] Kevin Höhle, Michael Kern, Timothy Hewson, and Rüdiger Westermann. A comparative study of convolutional neural network models for wind field downscaling. *Meteorological Applications*, 27(6):e1961, 2020.
- [21] Wenxuan Hu, Yvonne Scholz, Madhura Yeligi, Lueder von Bremen, and Ying Deng. Downscaling ERA5 wind speed data: A machine learning approach considering topographic influences. *Environmental Research Letters*, 18(9):094007, August 2023.
- [22] Louis Le Toumelin, Isabelle Gouttevin, Clovis Galiez, and Nora Helbig. A two-fold deep-learning strategy to correct and downscale winds over mountains. *Nonlinear Processes in Geophysics*, 31(1):75–97, February 2024.
- [23] Hai Lin, Jianping Tang, Shuyu Wang, Shuguang Wang, and Guangtao Dong. Deep learning downscaled high-resolution daily near surface meteorological datasets over East Asia. *Scientific Data*, 10(1):890, December 2023.
- [24] Ophélie Miralles, Daniel Steinfeld, Olivia Martius, and Anthony C. Davison. Downscaling of Historical Wind Fields over Switzerland Using Generative Adversarial Networks. *Artificial Intelligence for the Earth Systems*, 1(4), November 2022.
- [25] Tsuyoshi Thomas Sekiyama, Syugo Hayashi, Ryo Kaneko, and Ken-ichi Fukui. Surrogate Downscaling of Mesoscale Wind Fields Using Ensemble Superresolution Convolutional Neural Networks. *Artificial Intelligence for the Earth Systems*, 2(3), August 2023.
- [26] Nicolas Gasset, Ayrton Zadra, Frederic Dupont, Gérard Croteau, Jean-François Caron, Stephen Macpherson, Sylvain Heilliette, Josep Aparicio, Maziar Bani Shahabadi, Yves Rochon, Jacques Mont-Petit, Dorina Surcel Colan, Alain Caya, Charles Creese, Jean de Grandpré, Ron McTaggart-Cowan, and Alain Beaulne. Global Deterministic Prediction System (GDPS). Technical report, Environment and Climate Change Canada, December 2021.

- [27] Samuel Gilbert, Chantal Pic, Laurent Chardon, and Mike Neish. Global Environmental Multiscale (GEM) model. Environment and Climate Change Canada.
- [28] Thomas Milewski, Marc Verville, Danahé Paquin-Ricard, Dominik Jacques, and Jean-François Caron. High Resolution Deterministic Prediction System - National Domain (HRDPS-NAT). Technical report, Environment and Climate Change Canada, December 2021.
- [29] Ishaan Gulrajani, Faruk Ahmed, Martin Arjovsky, Vincent Dumoulin, and Aaron C Courville. Improved training of wasserstein gans. *Advances in neural information processing systems*, 30, 2017.
- [30] Christian Ledig, Lucas Theis, Ferenc Huszár, Jose Caballero, Andrew Cunningham, Alejandro Acosta, Andrew Aitken, Alykhan Tejani, Johannes Totz, Zehan Wang, et al. Photo-realistic single image super-resolution using a generative adversarial network. In *Proceedings of the IEEE Conference on Computer Vision and Pattern Recognition*, pages 4681–4690, 2017.
- [31] Olaf Ronneberger, Philipp Fischer, and Thomas Brox. U-net: Convolutional networks for biomedical image segmentation. In *Medical Image Computing and Computer-Assisted Intervention—MICCAI 2015: 18th International Conference, Munich, Germany, October 5-9, 2015, Proceedings, Part III 18*, pages 234–241. Springer, 2015.
- [32] Mehdi Mirza. Conditional generative adversarial nets. *arXiv preprint arXiv:1411.1784*, 2014.
- [33] Martin Arjovsky, Soumith Chintala, and Léon Bottou. Wasserstein generative adversarial networks. In *International Conference on Machine Learning*, pages 214–223. PMLR, 2017.
- [34] Manuel Fritsche, Shuhang Gu, and Radu Timofte. Frequency separation for real-world super-resolution. In *2019 IEEE/CVF International Conference on Computer Vision Workshop (ICCVW)*, pages 3599–3608. IEEE, 2019.
- [35] Haoyan Zhuang. xesmf: A python package for earth system modeling framework (esmf) regridding utilities, 2024. Version 0.8.8.
- [36] Nicolaas J Annau. DoWnGAN: Downscaling Wind Components Using Generative Adversarial Networks, 2022.
- [37] Johannes Schmude, Sujit Roy, Will Trojak, Johannes Jakubik, Daniel Salles Civitarese, Shraddha Singh, Julian Kuehnert, Kumar Ankur, Aman Gupta, Christopher E. Phillips, Romeo Kienzler, Daniela Szwarcman, Vishal Gaur, Rajat Shinde, Rohit Lal, Arlindo Da Silva, Jorge Luis Guevara Diaz, Anne Jones, Simon Pfreundschuh, Amy Lin, Aditi Sheshadri, Udaysankar Nair, Valentine Anantharaj, Hendrik Hamann, Campbell Watson, Manil Maskey, Tsengdar J. Lee, Juan Bernabe Moreno, and Rahul Ramachandran. Prithvi WxC: Foundation Model for Weather and Climate, September 2024.